1 **Large Scale Influences on Summertime Extreme Precipitation in the Northeastern United**

2 **States**

3

4

5   Allison B. Marquardt Collow[1,2], Michael G. Bosilovich[2], and Randal D. Koster[2]

6

7   [1]Universities Space Research Association, Columbia, Maryland and Goddard Earth Sciences

8   Technology and Research, Greenbelt, Maryland

9   [2]Global Modeling and Assimilation Office, NASA Goddard Space Flight Center, Greenbelt,

10   Maryland

11   Submitted to the *Journal of Hydrometeorology*

12

13   Corresponding Author:

14   Allison B. Marquardt Collow

15   Global Modeling and Assimilation Office, Code 610.1

16   NASA Goddard Space Flight Center

17   Greenbelt, Maryland 20771

18   Email: allison.collow@nasa.gov

19   Phone: 301-614-6653

20   Abstract

21   Observations indicate that over the last few decades there has been a statistically

22   significant increase in precipitation in the Northeastern United States and that this can be

23   attributed to an increase in precipitation associated with extreme precipitation events. Here we

24   use a state-of-the-art atmospheric reanalysis to examine such events in detail. Daily extreme

25   precipitation events defined at the 75th and 95th percentile from gridded gauge observations are

26   identified for a selected region within the Northeast. Atmospheric variables from the Modern Era

27   Retrospective Analysis for Research and Applications − Version 2 (MERRA-2) are then

28   composited during these events to illustrate the time evolution of associated synoptic structures,

29   with a focus on vertically integrated water vapor fluxes, sea level pressure, and 500 hPa heights.

30   Anomalies of these fields move into the region from the northwest, with stronger anomalies

31   present in the 95th percentile case. Although previous studies show tropical cyclones are

32   responsible for the most intense extreme precipitation events, only 10% of the events in this

33   study are caused by tropical cyclones. On the other hand, extreme events resulting from cut off

34   low pressure systems have increased. The time period of the study was divided in half to

35   determine how the mean composite has changed over time. An arc of lower sea level pressure

36   along the east coast and a change in the vertical profile of equivalent potential temperature

37   suggest a possible increase in the frequency or intensity of synoptic scale baroclinic disturbances.

1. Introduction

38

39   Observations indicate that extreme precipitation events have increased throughout the

40   contiguous United States (CONUS), with the largest increase in the northeast region of the

41   country (Janssen et al., 2014; Melillo et al., 2014; Agel et al., 2015; Frei et al., 2015). Flooding

42   associated with extreme precipitation events can result in economic losses and the loss of life,

43   which highlights the need for a complete understanding of such events. An improved

44   understanding of extreme precipitation events and how they will change in the future will help

45   enable the precautions needed to protect society from such events, e.g., through more accurate

46   forecasts.

47   While it is quite possible that the increasing trend in extreme precipitation events will

48   continue into the future, there is considerable uncertainty (IPCC, 2013; Janssen et al., 2014). The

49   frequency of extreme precipitation events in the Northeast varies by season, and this frequency

50   has changed over time. Significant increases in precipitation in the Northeast have been

51   documented in the fall and on an annual time scale (Kunkel et al., 2013), and a statistically

52   significant increase in extreme precipitation events has been documented during the Northeast

53   warm season (Frei et al., 2015). Many studies have shown that warmer air can hold more water

54   vapor, thereby increasing extreme rainfall; however the increase in extreme precipitation in the

55   Northeast has been shown to exceed that dictated by the Clausius-Clapeyron relationship

56   (Ivancic and Shaw, 2016).

57   Trends in observed precipitation and extreme precipitation events in the Northeastern

58   United States are further complicated by various meteorological causes that differ in frequency

59   depending on the season and region (Kunkel et al., 2012; Agel et al., 2015; Frei et al., 2015).

60   Extreme precipitation events in the Northeast have been shown to be caused by extratropical

61   cyclones, tropical cyclones, frontal systems, and mesoscale convective systems (Konrad, 2001;

62   Kunkel et al., 2012; Agel et al., 2015). Tropical cyclones tend to produce the most intense

63   summer and fall extreme precipitation events in the region, whereas frontal systems are the most

64   common cause for an extreme precipitation event during the summer and on an annual time scale

65   (Konrad, 2001; Kunkel et al. 2012); however varying spatial domains and definitions of an

66   extreme precipitation event produce a range of percentages of events caused by tropical cyclones

67   (Barlow, 2011; Kunkel et al., 2012; Agel et al., 2015). Fronts have been shown to be responsible

68   for the vast majority of annual precipitation in major storm track regions and 76% of annual

69   extreme precipitation events in the mid-latitudes (Catto et al., 2012; Catto and Pfahl, 2013).

70   While previous studies have documented the cause of extreme events in the Northeastern

71   United States, relatively little work has been done to evaluate the climatology of the synoptic

72   structures of these events and how such structures have changed over time in connection with the

73   increase of extreme precipitation. Here we examine these structures in detail, describing the

74   evolution of meteorological fields through the development and aftermath of extreme

75   precipitation events and contrasting, for example, the synoptic structures of weaker and stronger

76   precipitation events to determine what makes an event more extreme. Past studies have

77   suggested there is a weakening of atmospheric circulation during the summer months,

78   prolonging the duration of blocking systems (Coumou et al., 2015). As a result, quasi-stationary

79   patterns could be becoming common and therefore cause an increase in the frequency of extreme

80   precipitation events, which has already been documented in the Balkan Peninsula (Stadtherr et

81   al., 2016).

82   The datasets and methodology used for this study are provided in section 2. Section 3

83   focuses on the results; the section is subdivided to present a brief climatology of precipitation

84 and extreme precipitation events in the Northeastern United States, a composite analysis of

85 extreme precipitation events, an analysis of the impact of tropical cyclones and closed low

86 pressure systems on extreme precipitation events, and an indication of how the character of

87 extreme events has changed over time. A summary and discussion is provided in section 4.

88 **2. Data and Methods**

89 The primary tools for the analysis include observational and reanalysis products.

90 Observations of precipitation are from the Climate Prediction Center (CPC)'s gridded Unified

91 Gauge-Based Analysis of daily precipitation at a resolution of 0.25° by 0.25° (Xie et al. 2007;

92 Chen and Xie, 2008). The Modern-Era Retrospective Analysis for Research and Applications,

93 Version 2 (MERRA-2) was used to represent the large-scale circulation and meteorological

94 quantities that are not easily observed (Bosilovich et al. 2015; Gelaro et al. 2016, in prep).

95 Hourly data from MERRA-2 are available at a spatial resolution of 0.625° longitude by 0.5°

96 latitude, and daily averages ending at 12z were computed to match the temporal resolution of the

97 precipitation observations. MERRA-2 features additional observing systems and improvements

98 to the hydrological cycle not present in the original MERRA atmospheric reanalysis (Rienecker

99 et al. 2011), including the forcing of the land surface with observations-based precipitation fields

100 and the implementation of a moisture constraint, preventing an imbalance in global precipitation

101 and surface evaporation (Reichle and Liu, 2014; Takacs et al., 2016). MERRA-2 also features

102 numerous developments in the underlying model (Molod et al. 2015), such as in the surface layer

103 and boundary layer parameterizations and in the cumulus convection scheme. The data

104 assimilation has been updated to the latest Gridpoint Statistical Interpolation version and

105 includes global dry mass constraints that help minimize spurious temporal variability effects

106 (Takacs et al., 2016). Also, new observations not available to the original MERRA have been

107   added, such as GPS radio occultation and the Infrared Atmospheric Sounding Interferometer

108   (McCarty et al., 2016).

109   We focus in this paper on the northeastern United States region outlined in Figure 1, a

110   region that includes land areas between 40 and 45°N and 70 and 76°W. This region was selected

111   based on an analysis of the seasonal climatological means and interannual variability over the

112   past 30 years in an effort to reduce spatial variability in precipitation within the northeast region

113   as defined by the National Climate Assessment (Horton et al., 2014). Figures that were used to

114   further define the Northeast region can be seen in the supplemental document.

115   Using the CPC gauge observations, daily precipitation values for the area as a whole are

116   computed, and percentiles are then calculated from these spatial averages among the days with at

117   least 1 mm of precipitation, following Rivera et al. (2014), Hirata et al. (2015), and Westby et al.

118   (2015). The 1 mm threshold is used to ensure that only days with a precipitation event are

119   included in the percentile calculation. Keep in mind that the nature of our results will depend in

120   part on the area used here for the averaging; larger regions may favor widespread heavy

121   precipitation as opposed to local or regional extreme precipitation. Given the area we use, many

122   of the events we examine are widespread and on the synoptic scale, impacting most of the

123   region.

124   Percentiles were defined separately for each day of the year using a window around each

125   date of ±1 week and then considering together the daily precipitation values during the 2-week

126   period in each year from 1981 through 2010. This window around each date allows for more

127   robust statistics while maintaining any differences associated with seasonality. Warm and cold

128   season extreme precipitation events differ in frequency and intensity, and this methodology

129   allows for seasonal variations in precipitation to be taken into account (Frei et al., 2015). In this

130   study, we focus on June, July, and August.

131   Frei et al. (2015) classified extreme precipitation events using 90th, 95th, and 99th

132   percentiles, and the Climate Data Operators (CDO) and the Expert Team on Climate Change

133   Detection and Indices (ETCCDI; Alexander et al., 2006) classified them using 75th, 95th and 99th

134   percentiles. Here we focus on the 75th and 95th percentiles, with events falling into the category if

135   they are within a range of ±5 percentile units of the noted values. That is, the 75th percentile

136   grouping, or composite, does not include the more extreme events found in the 95th percentile

137   composite and can thus be considered a composite of relatively weaker events. By definition,

138   there are a similar number of events in both groupings (~200; see Table S1). This number is

139   representative of roughly 10% of the number of days with at least 1 mm of precipitation as

140   opposed to the total number of days within the time period due to the threshold used in the

141   percentile calculation. Note that such a compositing approach has been used to study events (e.g.,

142   atmospheric rivers) in other regions (Grotjahn and Faure, 2008; Warner et al., 2012; Gao et al.,

143   2014).

144   While MERRA-2 shows significant improvements over MERRA in the representation of

145   extreme precipitation events, there are still uncertainties associated with modeled precipitation

146   (Bosilovich et al., 2015). MERRA-2 and the CPC gauge data do not contain exactly the same

147   number of days above 1 mm to be included in the percentile calculations and therefore do not

148   result in the same number of events that exceed a given percentile. More importantly, there are a

149   number of dates that are considered extreme in the observations and not in MERRA-2, and vice

150   versa. As a result, only the observations are used here to determine whether an event falls in the

151   75th or 95th percentile categories. Using observations to determine extreme precipitation events

152   and reanalysis data for the large-scale circulation is a common methodology used in past studies

153   (eg. Gao et al., 2014).

3. Results

a. Climatology of the Northeastern United States

156   Having both mountains and a coastline, the climate in the Northeast is greatly influenced

157   by geography, and the region is susceptible to different varieties of weather including hurricanes,

158   extratropical cyclones, mesoscale systems, heat waves, and drought during the summer months.

159   Mean climate features during JJA over the period of 1980 through 2014 in MERRA-2 are shown

160   in Figure 1. Temperature at 2 m tends to decrease with increasing latitude (Figure 1a). Cooler

161   temperatures over the ocean inhibit daytime warming along the coast and higher elevations

162   associated with the Appalachian Mountains result in cooler temperatures, most notably over

163   eastern New York. The mountains also play a role in mean daily precipitation, with precipitation

164   enhanced over the higher elevation (Figure 1b).

165   The availability of moisture is a key component of precipitation events, and information

166   about this availability, e.g. in the form of vertically integrated water vapor flux, is a unique

167   feature of reanalyses such as MERRA-2. Tropospheric winds are generally from the west, with

168   maximum velocities centered around 45 °N (Figures S1 and S2), resulting in a mean eastward

169   transport of water vapor (Figure 1c). Vertically integrated moisture fluxes positioned over land

170   are also higher near the coast, most notably over Rhode Island and Cape Cod, Massachusetts,

171   with the Atlantic Ocean serving as a source of moisture. Moisture from the Atlantic Ocean can

172   also be seen in the total precipitable water vapor (TPW) along the coast (Figure 1d).

173   While summertime extreme precipitation frequency has changed over time in numerous

174   locations within the United States, the Northeast shows the largest increase in the frequency of

175   extreme events at the 95th percentile, according to the CPC Gauge observations (Figure 2). The

176   95th percentile used for Figure 2 was defined for each 0.25° by 0.25° grid box in the

177   observations. Most of the region has seen an increase greater than one such event per decade

178   (Figure 2a). The significance of the trend was evaluated using a Monte Carlo simulation; results

179   show that in many parts of the Northeast, the observed trend is significantly different from zero

180   at the 99% confidence level (Figure 2b).

181   A time series for area-averaged observed precipitation within the region of interest is

182   presented in Figure 3a (black curve). Based on a least squares regression and a Student-t test,

183   there is a statistically significant upward trend in mean precipitation over the 36-year time

184   period. A closer look at the time series indicates that the increase overtime is in fact

185   superimposed on an oscillation or a shift that occurs in the late 1990s; this might be related to the

186   Atlantic Multidecadal Oscillation, which has been shown to be positively correlated to

187   summertime precipitation and extreme precipitation in the Northeast United States (Enfield et al.,

188   2001; Curtis, 2008). It has been shown that the positive phase of the Atlantic Multidecadal

189   Oscillation leads to an area of decreased sea level pressure and a cyclonic circulation off the east

190   coast (Knight et al., 2006; Curtis, 2008). This cyclonic circulation is believed to increase the

191   flow of low level moisture into the region that is forced to rise due orographic lift from the

192   Appalachian Mountains, therefore leading to more frequent intense precipitation events.

193   While mean precipitation in the Northeast has increased over time, the median has not

194   (Figure 3a, red curve). This implies that while extreme precipitation events are increasing, non-

195   extreme events are not. This point is further emphasized in Figure 3b, which shows the time

196   series of 75th and 95th percentile precipitation events (in terms of number of events). While there

197   is considerable interannual variability in the number of 75th percentile precipitation events, their

198 frequency does not change over time. For the 95th percentile events, however, there is a steady

199 increase in number after the late 1990s, with a linear trend over the entire period that is

200 statistically significant at the 95% confidence interval.

201 *b. Composited Fields during Extreme Precipitation Events*

202 Using extreme precipitation events over the Northeast (as determined from the daily

203 gauge observations) as the basis for compositing, we compute composites of various

204 meteorological fields from MERRA-2. Total precipitation composited using the 75th and 95th

205 percentile Northeast precipitation events is shown in Figure 4. For both intensities, a wide area,

206 spanning the entire east coast, sees significant precipitation (on average) during these events. Our

207 methodology clearly pulls out large-scale events that cover an area much larger than the defined

208 Northeast region. The daily average precipitation may in fact capture precipitation from a system

209 that traveled through and impacted a different region earlier in the day. The composite based on

210 the 95th percentile indicates that the heaviest observed precipitation fell in the southern portion of

211 the Northeast region, along the coastline.

212 A key component of extreme precipitation events is the availability of moisture in the

213 region. Figure 5 shows the anomalous flow of moisture, more specifically, anomalies in the

214 vertically integrated water vapor flux, into the Northeast before, during, and after these events, as

215 represented by the two sets of composites. Values below 40 kg m^{-1} s^{-1} have been masked out to

216 draw attention to larger anomalies. From two days out there is little difference between

217 climatology and 75th percentile precipitation events, with the only anomaly being a hint of a

218 trough beginning to take shape in the Northern Great Plains and Midwest (Figure 5a). This

219 anomaly is amplified in magnitude and area in the 95th percentile composite, with the center

220 shifted to the south (Figure 5b). The day prior to an extreme precipitation event, the vertically

221   integrated moisture flux anomalies become stronger, forming a cyclonic circulation; again, the

222   cyclonic circulation is stronger and slightly farther south in the 95th percentile anomaly

223   composite (compare Figure 5c and d). Moisture flux anomalies are strongest in the southern

224   portion of the circulation. Anomalies are likely stronger to the south from the convergence of

225   moisture coming from the west and moisture from the Gulf of Mexico. The increased flow of

226   moisture from the Atlantic Ocean apparent in the 95th percentile composite for the day prior to

227   the event is somewhat deceptive. In that region, moisture fluxes in the composite are oriented

228   from the southwest but are smaller than what is seen in the climatology, and this is manifested in

229   the anomaly field as a change in direction that makes it look as if moisture is brought into the

230   region from the Atlantic Ocean (Figure S3).

231   On the day of the extreme precipitation event, the circulation pattern represented by the

232   vertically integrated moisture flux anomalies takes on an elongated shape, with a tilt from the

233   southwest to northeast (Figures 5e and f). The largest anomalies are now on the east side of the

234   circulation, with moisture being pulled in from the Atlantic Ocean in the warm conveyor belt of

235   enhanced southerly flow. Anomalies extend further south in the 95th percentile events, with

236   decreased moisture transport into Texas and Louisiana (Figure S3), and with an increased

237   westerly and southwesterly flow of moisture in the southeastern portion of the country. The Gulf

238   of Mexico serves as a moisture source for the 95th percentile composite but not so much for the

239   75th percentile composite. An additional difference between the 75th and 95th percentile events is

240   seen in the easterly anomalies over the Atlantic Ocean, which are absent during 75th percentile

241   events.

242   The day after the extreme precipitation event, the circulation pattern leaves the region

243   with a shift toward the northeast. For the 75th percentile composite, as the pattern nears the

244   Atlantic Ocean, the region of maximum moisture flux anomalies is broader than it was on the

245   day of the event.

246   As moisture is conveyed from the Gulf of Mexico and Atlantic Ocean, positive anomalies

247   of total precipitable water vapor (TPW) develop over the Northeast, as seen in Figure 6. TPW

248   anomalies are weak two days prior to an extreme precipitation event but become more significant

249   the day before the event. Maximum TPW anomalies are centered east of the Great Lakes in both

250   the 75th and 95th percentile cases; however, the anomalies are stronger for the latter composite.

251   The shape of the 75th percentile positive TPW anomaly is indicative of an extratropical cyclone,

252   whereas the 95th percentile anomaly appears broader. Relatively drier air develops to the west,

253   concurrent with the enhanced northerly flow. TPW anomalies are stronger on the day of the

254   event and become tilted from southwest to northeast, similar to what was seen with the vertically

255   integrated moisture flux anomalies. As the system exits the region the following day, the

256   magnitude of the anomaly does not decrease as the anomaly propagates eastward and moisture

257   becomes available from the Atlantic Ocean.

258   The anomalies of the vertically integrated water vapor flux provide some indication of the

259   overall flow in the troposphere during extreme precipitation events. However, wind anomalies in

260   the upper troposphere, in this case at 250 hPa, can also provide information regarding the

261   dynamics surrounding extreme precipitation events. This is illustrated in Figure 7. Anomalies

262   below 3 m s^{-1} have been masked out to highlight the more significant anomalies. In the

263   climatology (not shown), the strongest winds in the jet stream are located between 40 and 50 °N

264   with a general westerly flow. Two days prior to an extreme precipitation event, a stronger

265   meridional component of the 250 hPa winds is seen along the US-Canada border around

266   Montana and the Great Lakes. On the day before the event, these wind anomalies become

267   stronger and develop a cyclonic pattern centered around Minnesota. Wind speed divergence is

268   seen in the Midwest region, with directional divergence to the northeast along the border of

269   Ontario and Quebec. This divergence in the upper troposphere can signal convergence at the

270   surface and upward vertical motion in the column, a suitable component to an extreme

271   precipitation event.

272   The strongest 250 hPa wind anomalies are present on the day of the extreme precipitation

273   event, with maxima in the northwest quadrant of the selected Northeast region. The entire region

274   is located in the right entrance region of enhanced upper level winds, where upward vertical

275   motion occurs. These maxima in the anomaly fields are oriented toward the northeast in the 75th

276   percentile events but have a more northward orientation in the 95th percentile events.

277   Two days prior to an extreme precipitation event, a trough develops upstream of the

278   region of interest in both the 75th and 95th percentile composites of 500 hPa heights (Figure 8a

279   and b). The negative height anomaly is generally stronger and located slightly to the south in the

280   95th percentile case. In both cases the trough is embedded in a wave train oriented east to west.

281   The trough tracks to the southeast with movement slowing between the day of and the day after

282   an extreme precipitation event.

283   Notice in Figure 8 that the low-high dipoles around the event are stronger in magnitude

284   for the 95th percentile composite. The negative anomaly in 500 hPa height is accompanied by a

285   similar pattern in sea level pressure anomalies, though the low pressure system is not vertically

286   stacked (Figure 9). The positive anomaly to the east of the negative anomaly at 500 hPa develops

287   coherently with the low in sea level pressure in the 95th percentile composite, but not in the 75th.

288   Negative sea level pressure anomalies become elongated the day of the event and the day after

289   the event. The shape of the negative sea level pressure anomaly, particularly in the 95th percentile

290   case the day after the event, resembles a low pressure system and trailing cold front.

291   A reduction in cut off lows has been shown to be responsible for a reduction in

292   precipitation in southern Australia, and a change in blocking patterns could cause the opposite

293   response in the United States (Risbey et al., 2013). Following the methodology of Pook et al.

294   (2006), an event was determined to be caused by a cut off low if MERRA-2 indicated a closed

295   area of sea level pressure below 1008 hPa with a trough at 500 hPa, or a closed contour in 500

296   hPa height, alongside a negative anomaly in 1000 hPa to 500 hPa thickness of at least 20 m

297   compared to climatology within the synoptic region. The number of 95th percentile extreme

298   precipitation events related to cut off lows as a function of year is shown in Figure 10a, along

299   with the time series of the total number of extreme events. While there is a statistically

300   significant increasing trend in events caused by a cut off low, this trend is not large enough to

301   account for the total observed increase in extreme precipitation events in the Northeast. On the

302   other hand, despite year-to-year variability, there is no change over time in the number of 75th

303   percentile events caused by cut off lows.

304   *d. Tropical Extreme Precipitation Events*

305   Previous studies of extreme precipitation events in the Northeast indicate that the

306   percentage of summertime extreme events caused by tropical cyclones can exceed 25% (Kunkel

307   et al., 2012; Agel et al., 2015). This number is very dependent on the methodology used to define

308   an extreme event and a tropical cyclone. Following Kunkel et al. (2012), we define an extreme

309   Northeast event to be caused by a tropical cyclone if a storm listed in the National Hurricane

310   Center's North Atlantic hurricane database (HURDAT) was within 5° of the Northeast region.

311   Given our definition of an extreme event as falling within plus or minus 5 percentile units of the

312   95th percentile, we find the percentage of extreme precipitation events in JJA caused by a tropical

313   cyclone to be a relatively low 10.6%, though we are focusing on a smaller region than in the

314   previous studies and are using percentile based approach to define events. In contrast, Kunkel et

315   al. (2012) use a threshold (which does not vary with time of year) to define events based on a

316   return period of five years, and they areal average the number of events caused by tropical

317   cyclones for a larger spatial area, one that spans Maine through West Virginia.

318   Most of the extreme events we have linked to tropical cyclones are in the more recent

319   time period; only two occur in the 1980s (Figure 11a), and both of these events are related to

320   tropical storm Chris, which traveled through the region in 1988 as a tropical depression. There is

321   no significant linear trend in the time series of events caused by tropical cyclones during 1985-

322   2014, as there are never more than two events in a given year. The total number of extreme

323   precipitation events per year, on the other hand, does have a statistically significant trend (Figure

324   3b).

325   The average intensity of an event is somewhat determined by the methodology used to

326   define an event, and this intensity hovers around 20 mm day^{-1} for all events (Figure 11b). Aside

327   from 2011 and 2013, which saw nearly doubled intensities due to Hurricane Irene and Tropical

328   Storm Andrea, the average intensity of the tropical cyclone-related events is roughly the same.

329   The total seasonal precipitation from extreme events (Figure 11c) is thus more closely related to

330   the number of events than their intensity. There are a number of years without any hurricanes but

331   with a high total accumulation from extreme events (e.g., 1982, 1998, and 2006). While the

332   largest accumulation from extreme events occurred in 2011, coinciding with the maximum

333   average intensity due to tropical cyclones, overall there is no statistically significant indication

334   that tropical cyclones are responsible for the increase in extreme precipitation events in the

335   Northeast.

336   When events caused by a tropical cyclone are removed from the 95th percentile events,

337 the composited sea level pressure and 500 hPa heights on the day of the extreme precipitation

338 events (not shown) do not change much from those seen in Figures 8f and 9f. This is likely due

339 to the fact that only a small fraction of events were removed – only 21 out of ~200 95th percentile

340 precipitation events between 1980 and 2014 matched a tropical cyclone in HURDAT. Figure 12

341 shows the sea level pressures composited on these 21 cyclone-related events. (Note that there

342 were not enough events in the 75th percentile category to allow a corresponding analysis.)

343 Leading up to the day of an extreme precipitation event, an area of suppressed sea level pressure

344 can be seen coming up the coast rather than moving in from the northwest, as in Figure 9 (for all

345 95th percentile events). There is a wider trough in sea level pressure for the tropical cyclone-

346 related events, though caution must be taken with a direct comparison due to the fact that the

347 different composites are based on a different number of events. One commonality between

348 Figures 9 and 12 is the region of a positive sea level pressure anomaly to the northeast, helping

349 to steer the region of low pressure.

350 *e. Change in Composites Over Time*

351   To examine factors that may induce changes in extreme precipitation over time, we

352 compare composites from the first half of the MERRA-2 time period (1980 though 1996) to

353 those constructed from the second half (1997 through 2014) using the same time series of

354 extreme events as the previous composites. Time difference composites (later period minus early

355 period) for sea level pressure, 500 hPa heights, vertically integrated moisture fluxes,

356 precipitation, Eady growth rate, and a vertical cross section of equivalent potential temperature

357 on the day of a 95th percentile precipitation event are shown in Figure 13. Note that in contrast to

358 the previous figures, which showed anomalies relative to climatology, Figure 13 shows the

359   difference in the total fields between the two time periods. Most of the United States saw a

360   decrease in sea level pressure, though the only region with a statistically significant decrease

361   extends from Maine through northeastern Florida (Figure 13a). The shape of this statistically

362   significant region is reminiscent of a cold front with the northern edge over the eastern half of

363   the selected region, but this can also be indicative of cut off lows or extratropical cyclones. Cold

364   fronts are a significant contributor to summertime extreme precipitation events in the Northeast

365   (Kunkel et al., 2012) and are a potential factor towards the observed increase in extreme

366   precipitation events.

367   A region of reduced 500 hPa height during 95th percentile events is also present in the

368   later period (Figure 13b). It was shown earlier that events are not vertically stacked, and this is

369   also indicated by the time difference plots. The region of decreased 500 hPa height lies to the

370   west of the region of decreased sea level pressure, and it also lies to the south, perhaps indicating

371   that more events are taking a track more analogous to a nor'easter rather than an Alberta clipper.

372   An area of statistically significant higher heights is located to the northeast, showing an increase

373   in the pressure gradient over time during extreme precipitation events. Moisture fluxes have also

374   strengthened, particularly over the Gulf Stream (Figure 13c).

375   In agreement with the trends seen in Figure 2, the time differenced composite of observed

376   precipitation during 95th percentile events shows an increase through the eastern portion of New

377   York (Figure 13d). On the other hand, Connecticut, Rhode Island, and Massachusetts have

378   experienced a decrease in this extreme precipitation. Apparently, during the second half of the

379   evaluated time period, the events identified as extreme according to the area-averaged

380   precipitation tended to occur farther to the west, increasing the precipitation in New York and

381   decreasing the precipitation near the coast. This is somewhat in agreement with Figure 2, which

382   does not show a significant trend in extreme precipitation events in Massachusetts, Connecticut,

383   or Rhode Island.

384   Baroclinic instability can be a measure of the potential for "storminess" within a region,

385   and one metric for this is the Eady growth rate (Hoskins and Valdes, 1990). The change in the

386   maximum Eady growth rate, computed for the layer of 700 to 300 hPa, between 1980 though

387   1996 and 1997 through 2014 during 95th percentile precipitation events is shown in Figure 13e.

388   The northern edge of the region overlaps a strip of decreased Eady growth rate over time, while

389   there is an increase to the south. This may indicate a southward shift in storm tracks.

390   Extratropical cyclones are typically located further north in the summer compared to the winter;

391   a southerly shift in Eady growth rate in the summer, however, would indicate that the region

392   could experience more events related to extratropical systems. The statistically significant

393   increase in Eady growth rate just south of the region would place an extratropical cyclone in an

394   ideal location for an onshore flow of moisture into the region along with the dynamics required

395   for precipitation to develop. A comparison to future projections of Eady mean growth rate can be

396   seen in the supplemental material.

397   In order to determine if there is a thermodynamic component to the observed changes

398   related to extreme precipitation events, a cross section of the vertical profile of equivalent

399   potential temperature, θ_e, and specific humidity at 42 N was analyzed. A constant latitude was

400   chosen through the center of the region. An increase in θ_e, as indicated by red shading in Figure

401   13f, and specific humidity, indicated by solid black contours, over time can be seen at the surface

402   over the region. These increases slant eastward with increasing height and extend through 300

403   hPa for θ_e ; however, humidity is confined to a shallower region within the troposphere. Cooler

404   and drier air lags behind, aside from the increase in θ_e in the upper troposphere. The eastward

405 slant with height in thermodynamic properties furthers the suggestion of an increase in extreme

406 precipitation events associated with frontal activity, though additional work is needed to fully

407 determine if the frequency or intensity of frontal systems have changed over time.

408 **4. Summary and Discussion**

409 Extreme precipitation events can have large impacts on society, and observations indicate

410 that these events have increased during the months of June, July, and August in the Northeastern

411 United States. This increase in extreme precipitation events is statistically significant and is the

412 largest and most widespread change in extreme precipitation in the United States. Based on

413 future climate projections, it is possible this trend will continue, sparking the need for a greater

414 understanding of the details surrounding extreme precipitation events in the Northeast (IPCC,

415 2013; Janssen et al., 2014).

416 In this paper, we examine in detail the character of meteorological fields associated with

417 extreme precipitation events in the Northeast. With observational precipitation records, we

418 construct composites from MERRA-2 of general circulation and synoptic structure leading up to,

419 during, and following extreme precipitation events. Overall, the composites provide evidence of

420 extratropical cyclones that pass through the Northeastern United States and produce large

421 amounts of rainfall, with stronger anomalies in dynamical quantities seen for the 95th percentile

422 events. Lower pressures at the surface and divergence aloft allow for upward vertical motion,

423 while the flow around the low pressure area and the high pressure to the east from the associated

424 wave train conveys moisture into the region sufficient enough for heavy rainfall.

425 Previous studies show the summer time atmospheric circulation has weakened, with an

426 increase greater than 40% in high amplitude days in 500 hPa height contours during July,

427   August, and September (Francis and Vavrus, 2015; Francis and Skific 2015) and an increase in

428   JJA North Atlantic blocking events (Barnes et al, 2014; Hanna et al., 2015; Hanna et al., 2016).

429   As a result, in combination with the trend in Eady growth rate, baroclinic systems that produce

430   extreme events are becoming more stationary. With the Atlantic Ocean providing a vast moisture

431   supply, and with the increasing occurrence of quasi-stationary low pressure systems and frontal

432   systems, extreme precipitation events in the Northeast have become more common. These

433   dynamics have also been demonstrated in studies looking at blocking high pressure systems in

434   relation to Arctic Amplification (Coumou et al., 2015). Dynamical changes in addition to the

435   "wet gets wetter" theory and the ability of warmer air to hold more moisture are likely

436   contributors to the increase in extreme precipitation.

437   Note that convective events are not well represented in our composites. In this paper we

438   identify extreme events by considering precipitation averaged over the Northeast area outlined in

439   Figure 1, and this area is substantially larger than the spatial scale of individual convective

440   events. In effect, our analysis focuses by construction on large-scale events and the associated

441   character of the large-scale circulation. In addition, by using daily averages of meteorological

442   fields, we further average out characteristics of events that are not caused by large-scale,

443   synoptic features.

444   There is, of course, still much we can learn about extreme precipitation events in the

445   Northeast using these techniques. There are indications, for example, that extreme events

446   stemming from frontal systems should be separated in our compositing analysis from those

447   associated with extratropical cyclones, given that fronts are a leading cause of summertime

448   extreme precipitation events (Kunkel et al., 2012; Catto and Pfahl, 2013), in order to further

449   explore the nature of frontal systems and their connection to the changing extreme precipitation.

450 Also, while our composites show little change when tropical cyclones are removed, this does not

451 necessarily mean that tropical cyclones are not contributing to the increase in extreme

452 precipitation events; it only says that a small percentage of summertime events are caused by

453 tropical cyclones. Using reanalysis data to composite extreme events with a full classification of

454 the underlying systems that generate the extreme rainfall should provide useful information.

455 *Acknowledgments*

462 **5. References**

463 Agel, L., M. Barlow, J. H. Qian, F. Colby, E. Douglas, and T. Eichler, 2015: Climatology of

464 daily precipitation and extreme precipitation events in the Northeast United

465 States, *Journal of Hydrometeorology*, **16**, 2537-2557, doi:

466 *http://dx.doi.org/10.1175/JHM-D-14-0147.1*.

467 Alexander, L. V., and Coauthors, 2006: Global observed changes in daily climate extremes of

468 temperature and precipitation. *J. Geophys. Res.*, **111**, D05109, doi:

469 10.1029/2005JD006290.

470 Barlow, M., 2011: Influence of hurricane-related activity on North American extreme

471 precipitation, *Geophys. Res. Lett.*, **38**, L04705, doi:10.1029/2010GL046258.

472   Barnes, E. A., E. Dunn-Sigouin, G. Masato and T. Woollings, 2014: Exploring recent trends in

473   Northern Hemisphere blocking. *Geophysical Research Letters*, **41**,

474   doi: 10.1002/2013GL058745.

475   Bosilovich, M. G., et al., 2015: MERRA-2: Initial evaluation of the climate, *Technical Report*

476   *Series on Global Modeling and Data Assimilation*, **43**, NASA/TM-2015-104606.

477   Catto, J. L., C. Jakob, G. Berry, and N. Nicholls, 2012: Relating global precipitation to

478   atmospheric fronts, *Geophys. Res. Lett*., **39**, L10805, doi:10.1029/2012GL051736.

479   Catto, J. L., and S. Pfahl, 2013: The importance of fronts for extreme precipitation, *J. Geophys.*

480   *Res. Atmos*., **118**, 10,791–10,801, doi:10.1002/jgrd.50852.

481   Chen, M., and P. Xie, 2008: CPC Unified Gauge-based Analysis of Global Daily Precipitation,

482   Western Pacific Geophysics Meeting, 29 July – 1 August 2008, Cairns, Australia.

483   Coumou, D., J. Lehmann, and J. Beckmann, 2015: The weakening summer circulation in the

484   Northern Hemisphere mid-latitudes. *Science*, **348**, 324-327, doi:

485   10.1126/science.1261768.

486   Curtis, S., 2008: The Atlantic multidecadal oscillation and extreme daily precipitation over the

487   US and Mexico during the hurricane season. *Clim. Dyn.,* **30**, 343-351, doi:

488   10.1007/s00382-007-0295-0.

489   Enfield, D.B., A.M. Mestas-Nuñez, and P.J. Trimble, 2001: The Atlantic Multidecadal

490   oscillation and its relation to rainfall and river flows in the continental US. *Geophysical*

491   *Research Letters*, **28**, 2077-2080, doi: 10.1029/2000GL012745.

492   Francis, J. A. and S. J. Vavrus, 2015: Evidence for a wavier jet stream in response to rapid Arctic

493   warming. *Environmental Research Letters*, **10**, doi:10.1088/1748-9326/10/1/014005.

494   Francis, J.A. and N. Skific, 2015: Evidence linking rapid Arctic warming to mid-latitude weather

495   patterns. *Phil. Trans. R. Soc*. A, **373**, doi:10.1098/rsta.2014.0170.

496   Frei, A. K. E. Kunkel, and A. Matonse, 2015: The seasonal nature of extreme hydrological

497   events in the Northeastern United States. *J. Hydrometeor*, **16**, 2065–2085, doi:

498   http://dx.doi.org/10.1175/JHM-D-14-0237.1.

499   Gao, X., C. A. Schlosser, P. Xie, E. Monier, and D. Entekhabi, 2014: An analogue approach to

500   identify heavy precipitation events: Evaluation and application to CMIP5 climate models

501   in the United States. *J. Clim*, **27**, 5941–5963, doi: http://dx.doi.org/10.1175/JCLI-D-13-

502   00598.1.

503   Gelaro, R. and co-authors, 2016: The MERRA-2 Project. In Preparation for *J. Clim*.

504   Grotjahn, R. and G. Faure, 2008: Composite predictor maps of extraordinary weather events in

505   the Sacramento, California, Region*. *Weather and Forecasting*, **23**, 313-335, doi:

506   http://dx.doi.org/10.1175/2007WAF2006055.1.

507   Hanna, E., T. E. Cropper, P. D. Jones, A. A. Scaife, and R. Allan, 2015: Recent seasonal

508   asymmetric changes in the NAO (a marked summer decline and increased winter

509   variability) and associated changes in the AO and Greenland Blocking Index. *Int. J.

510   Climatol*, **35**, 2540–2554. doi:10.1002/joc.4157.

511   Hanna, E., T. E. Cropper, R. J. Hall, and J. Cappelen, 2016: Greenland Blocking Index 1851–

512   2015: a regional climate change signal. *Int. J. Climatol*., in press, doi:10.1002/joc.4673.

513   Horton, R., G. Yohe, W. Easterling, R. Kates, M. Ruth, E. Sussman, A. Whelchel, D. Wolfe, and

514   F. Lipschultz, 2014: Ch. 16: Northeast. Climate change impacts in the United States: The

515   Third National Climate Assessment, J. M. Melillo, Terese (T.C.) Richmond, and G. W.

516   Yohe, Eds., *U.S. Global Change Research Program*, 16-1-nn.

517   Hirata, F. E. and A. M. Grimm, 2015: The role of synoptic and intraseasonal anomalies in the

518   life cycle of summer rainfall extremes over South America. *Climate Dynamics*, in press,

519   doi: 10.1007/s00382-015-2751-6.

520   Hoskins, B. J. and P. J. Valdes, 1990: On the existence of storm-tracks. *J. Atoms. Science*, **47**,

521   1854-1864, doi: 10.1175/1520-0469(1990)047<1854:OTEOST>2.0CO;2.

522   IPCC, 2013: Summary for Policymakers. In: Climate Change 2013: The Physical Science Basis.

523   Contribution of Working Group I to the Fifth Assessment Report of the

524   Intergovernmental Panel on Climate Change [Stocker, T.F., D. Qin, G.-K. Plattner, M.

525   Tignor, S.K. Allen, J. Boschung, A. Nauels, Y. Xia, V. Bex and P.M. Midgley (eds.)].

526   Cambridge University Press, Cambridge, United Kingdom and New York, NY, USA.

527   Ivancic, T. J., and S. B. Shaw, 2016: A US-based analysis of the ability of the Clausius-

528   Clapeyron relationship to explain changes in extreme rainfall with changing

529   temperature. *J. Geophys. Res. Atmos.*, **121**, 3066-3078, doi: 10.1002/2015JD024288.

530   Janssen, E., D. J. Wuebbles, K. E. Kunkel, S. C. Olsen, and A. Goodman, 2014: Observational-

531   and model-based trends and projections of extreme precipitation over the contiguous

532   United States, *Earth's Future*, **2**, doi:10.1002/2013EF000185.

533   Knight, J. R., C. K. Folland, and A. A. Scaife, 2006: Climate impacts of the Atlantic

534   Multidecadal Oscillation, *Geophys. Res. Lett.*, **33**, L17706, doi:10.1029/2006GL026242.

535   Konrad II, C. E., 2001: The Most Extreme Precipitation Events over the Eastern United States

536   from 1950 to 1996: Considerations of Scale. *J. Hydrometeor*, **2**, 309–325, doi:

537   10.1175/1525-7541(2001)002<0309:TMEPEO>2.0.CO;2.

538   Kunkel, K. E., D. R. Easterling, D. A. R. Kristovich, B. Gleason, L.Stoecker, and R. Smith,

539   2012: Meteorological causes of the secular variations in observed extreme precipitation

540   events for the Conterminous United States. *J. Hydrometeor*, **13**, 1131–1141, doi:

541   http://dx.doi.org/10.1175/JHM-D-11-0108.1.

542   Kunkel, K. E. and Coauthors, 2013: Regional climate trends and scenarios for the U.S. National

543   Climate Assessment: Part 1. Climate of the Northeast U.S. NOAA Tech. Rep. NESDIS

544   142-1, 80pp.

545   McCarty, W., and co-authors, 2016: MERRA-2 Input Observations: Summary and Initial

546   Assessment, *Technical Report Series on Global Modeling and Data Assimilation*, **45**,

547   NASA/TM-2016-104606, in preparation.

548   Melillo, J. M., T. C. Richmond, and G. W. Yohe, 2014: Ch. 2: Our Changing Climate. *Climate*

549   *Change Impacts in the United States: The Third National Climate Assessment*, U.S.

550   Global Change Research Program, 19-67. doi:10.7930/J0KW5CXT.

551   Molod, A., L. Takacs, M. Suarez, M., J. and Bacmeister, 2015: Development of the GEOS-5

552   atmospheric general circulation model: evolution from MERRA to MERRA2, *Geosci.*

553   *Model Dev.*, **8**, 1339-1356, doi:10.5194/gmd-8-1339-2015.

554   Pook, M. J., P. C. McIntosh, and G. A. Meyers, 2006: The Synoptic Decomposition of Cool-

555   Season Rainfall in the Southeastern Australian Cropping Region, *Journal of Applied*

556   *Meteorology and Climatology*, **45**, 1156-1170, doi: 10.1175/JAM2394.1.

557   Reichle, R. H., and Q. Liu, 2014: Observation-corrected precipitation estimates in GEOS-5.

558   *NASA/TM–2014-104606*, Vol. **35.**

559   Rienecker, M. M., and Co-Authors, 2011: MERRA, NASA's Modern-Era Retrospective

560   Analysis for Research and Applications. *J. Climate*, **24**, 3624-3648, doi:

561   http://dx.doi.org/10.1175/JCLI-D-11-00015.1.

562   Risbey, J. S., P. C. McIntosh, and M. J. Pook, 2013: Synoptic components of rainfall variability

563   and trends in southeast Australia. *Int. J. Climatol.*, **33**, 2459–2472, doi:10.1002/joc.3597.

564   Rivera, E. R., F. Dominguez, and C. L. Castro, 2014: Atmospheric rivers and cool season

565   extreme precipitation events in the Verde River Basin of Arizona. *J. Hydrometeor*, **15**,

566   813–829, doi: http://dx.doi.org/10.1175/JHM-D-12-0189.1.

567   Stadtherr, L., D. Coumou, V. Petoukhov, S. Petri, and S. Rahmstorf, 2016: Record Balkan floods

568   of 2014 linked to planetary wave resonance. *Science Advances*, **2**, e1501428, doi:

569   10.1126/sciadv.1501428.

570   Takacs, L.L., M.J. Suárez, and R. Todling, 2016: Maintaining atmospheric mass and water

571   balance in reanalyses. *Quart. J. Roy. Meteor. Soc.*, accepted, doi: 10.1002/qj.2763.

572   Warner, M. D., C. F. Mass, and E. P. Salathé Jr., 2012: Wintertime extreme precipitation events

573   along the Pacific Northwest coast: Climatology and synoptic evolution. *Mon. Wea. Rev.*,

574   **140**, 2021–2043, doi: http://dx.doi.org/10.1175/MWR-D-11-00197.1.

575   Westby, R. M., R. X. Black, 2015: Development of anomalous temperature regimes over the

576   Southeastern United States: Synoptic behavior and role of low-frequency modes.

577   *Weather and* Forecasting, **30**, 553-570, doi: http://dx.doi.org/10.1175/WAF-D-14-

578   00093.1.

579   Xie, P., A. Yatagai, M. Chen, T. Hayasaka, Y. Fukushima, C. Liu, and S. Yang, 2007: A gauge-

580   based analysis of daily precipitation over East Asia, *J. Hydrometeorol.*, **8**, 607-626, doi:

581   http://dx.doi.org/10.1175/JHM583.1.
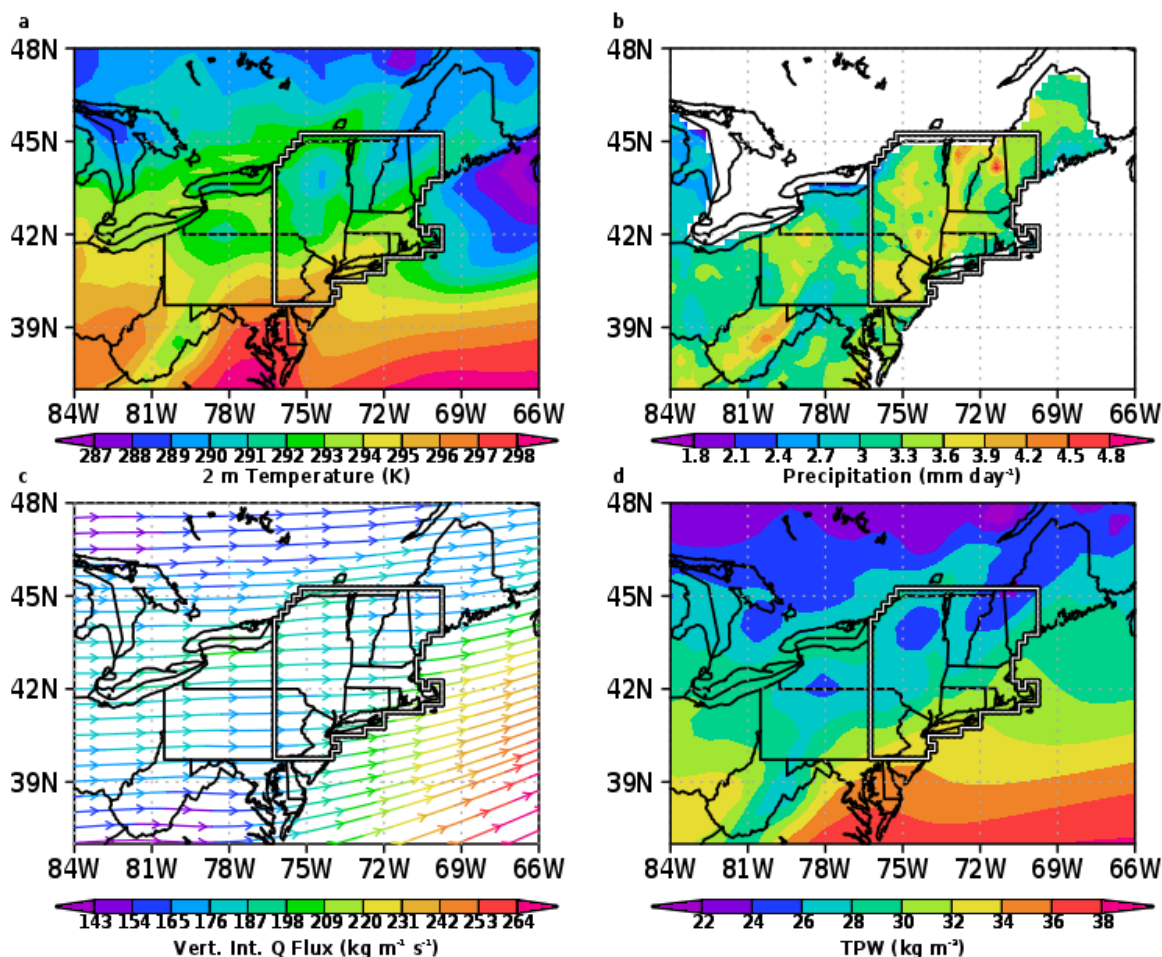
582

583   **6. Figure Captions**

584   Figure 1: Mean June, July, and August (a) 2 m temperature, (b) precipitation, (c) vertically

585   integrated water vapor fluxes, and (d) total precipitable water vapor over the period of 1980

586   through 2014. The Northeast region as defined in this study is outlined in black.

587   Figure 2: (a) Trend in the number of June, July, and August precipitation events at the 95th

588   percentile (b) Significance of the trend in (a) as calculated using a Monte Carlo simulation.

589   Figure 3: (a) Area averaged mean and median observed precipitation in the Northeast United

590   States during June, July, and August from 1979 through 2014, (b) The number of 75th and 95th

591   percentile precipitation events in the Northeast United States during June, July, and August.

592   Trends calculated with a least squares progression are given in parentheses and asterisks indicate

593   statistical significance at a 95% confidence interval.

594   Figure 4: Observed precipitation composited during (a) 75th percentile events and (b) 95th

595   percentile events.

596   Figure 5: Vertically integrated water vapor flux anomalies composited from two days prior to

597   one day after an observed 75th (left column) and 95th (right column) percentile precipitation

598   event. Anomalies below 40 kg m^{-1} s^{-1} are masked out.

599   Figure 6: Total precipitable water vapor anomalies composited from two days prior to one day

600   after an observed 75th (left column) and 95th (right column) percentile precipitation event.

601   Hatching denotes regions with a statistical significance of 95%.

602   Figure 7: 250 hPa wind anomalies composited from two days prior to one day after an observed

603   75th (left column) and 95th (right column) percentile precipitation event. Anomalies below

604   3 m s^{-1} are masked out.

605   Figure 8: 500 hPa height anomalies composited from two days prior to one day after an observed

606   75th (left column) and 95th (right column) percentile precipitation event. Hatching denotes

607   regions with a statistical significance of 95%.

608   Figure 9: Sea level pressure anomalies composited from two days prior to one day after an

609   observed 75th (left column) and 95th (right column) percentile precipitation event. Hatching

610   denotes regions with a statistical significance of 95%.

611   Figure 10: Time series of the number of total events and those caused by a cut off low for the (a)

612   95th percentile and (b) 75th percentile.

613   Figure 11: (a) Time series of number of total and tropical 95th percentile events in the Northeast

614   during June, July, and August. (b) Time series of the average intensity of a 95th percentile event

615   in the Northeast during June, July, and August. (c) Time series of the total amount of

616   precipitation from a 95th percentile event for all events and those caused by a tropical cyclone in

617   the Northeast during June, July, and August.

618   Figure 12: Sea level pressure anomalies composited from two days prior to one day after a 95th

619   percentile precipitation event caused by a tropical cyclone. Hatching denotes regions with a

620   statistical significance of 95%.

621   Figure 13: The difference in (a) sea level pressure, (b) 500 hPa height, (c) vertically integrated

622   moisture flux, (d) observed precipitation, (e) Eady growth rate, and (f) the vertical profile of

623   equivalent potential temperature at 42 N composites during 95th percentile precipitation events

624   calculated by subtracting the mean composite for 1980 through 1996 from the composite for

625   1997 through 2014. Hatching denotes regions with a statistical significance of 95%.

626   **Figures**

627

628   Figure 1: Mean June, July, and August (a) 2 m temperature, (b) precipitation, (c) vertically

629   integrated water vapor fluxes, and (d) total precipitable water vapor over the period of 1980

630   through 2014. The Northeast region as defined in this study is outlined in black.

631

632
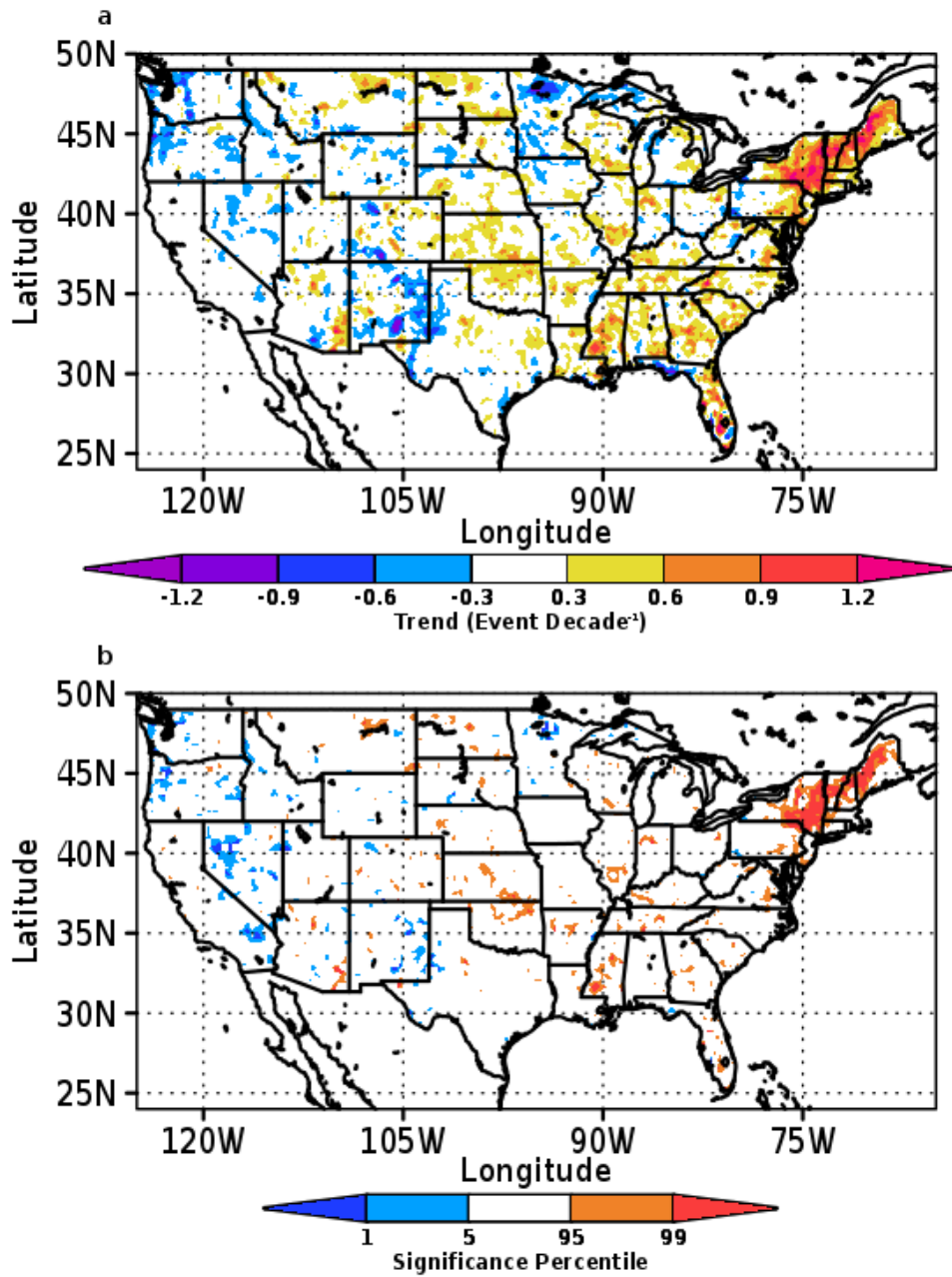
633

634   Figure 2: (a) Trend in the number of June, July, and August precipitation events at the 95th

635   percentile (b) Significance of the trend in (a) as calculated using a Monte Carlo simulation.
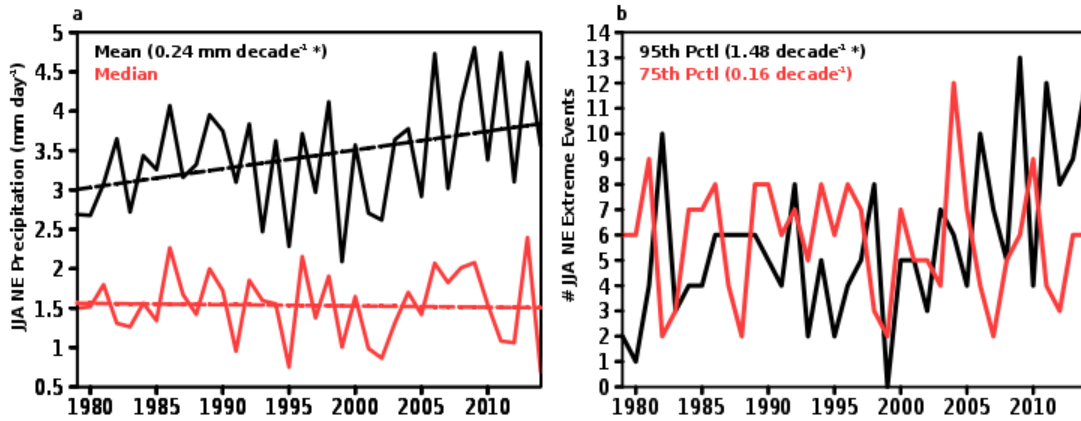
636

637   Figure 3: (a) Area averaged mean and median observed precipitation in the Northeast United

638   States during June, July, and August from 1979 through 2014, (b) The number of 75th and 95th

639   percentile precipitation events in the Northeast United States during June, July, and August.

640   Trends calculated with a least squares progression are given in parentheses and asterisks indicate

641   statistical significance at a 95% confidence interval.

642

643
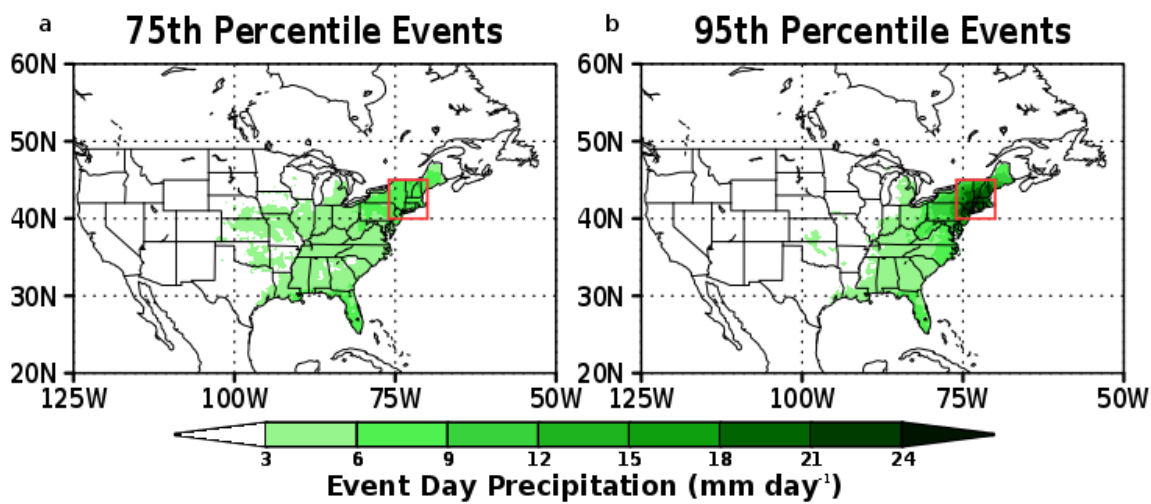
644

645   Figure 4: Observed precipitation composited during (a) 75th percentile events and (b) 95th
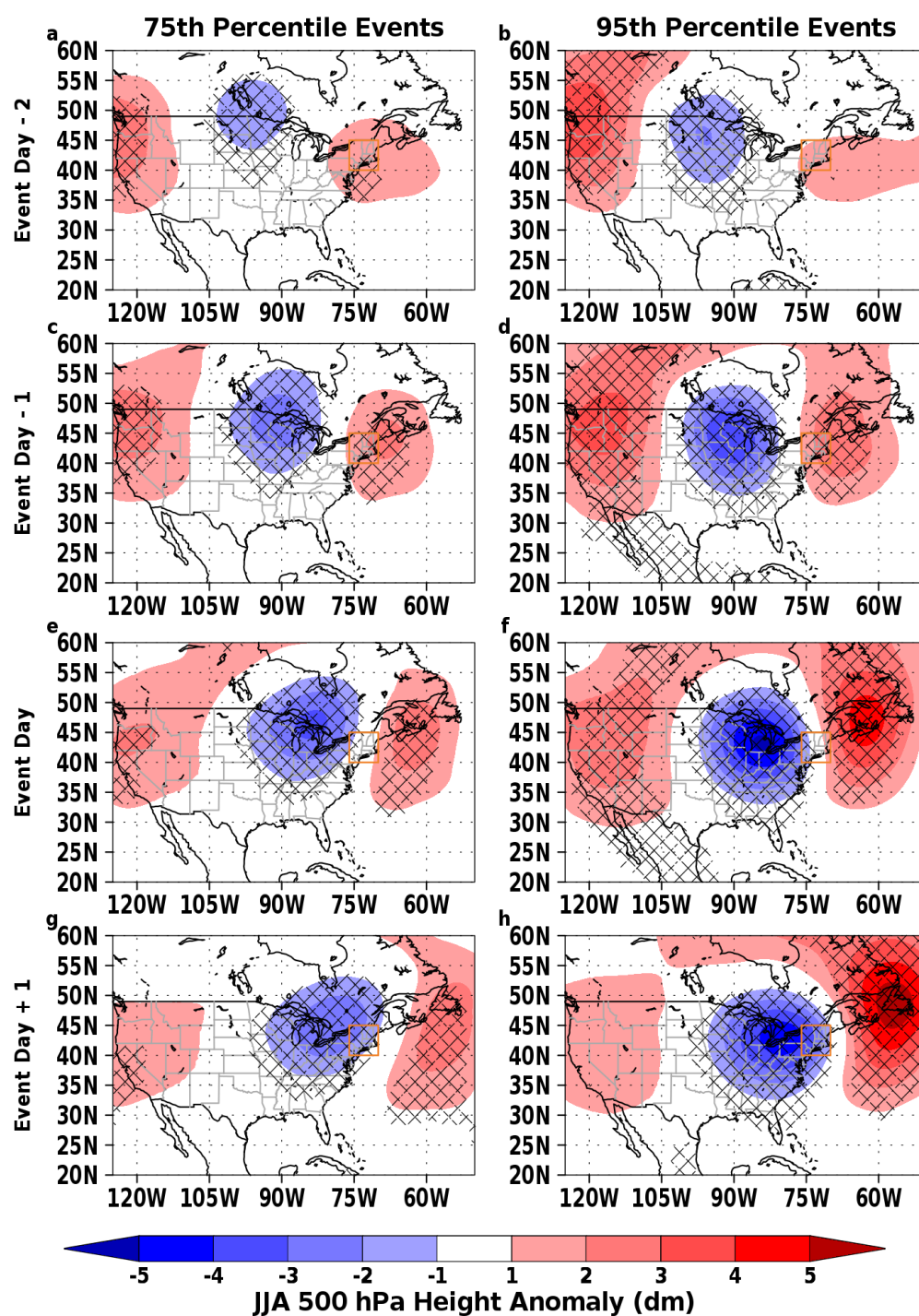
646   percentile events.
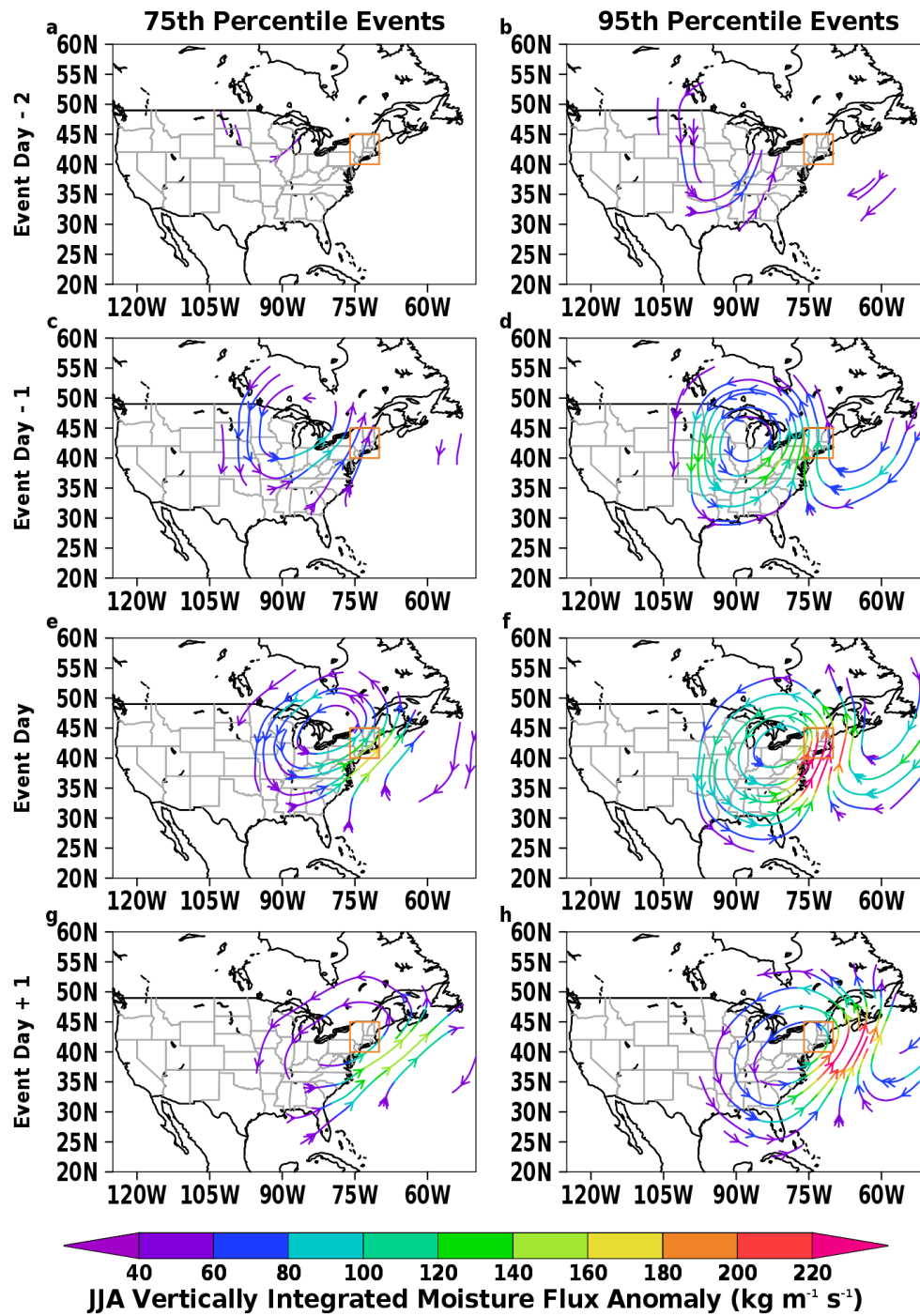
Figure 5: Vertically integrated water vapor flux anomalies composited from two days prior to one day after an observed 75th (left column) and 95th (right column) percentile precipitation event. Anomalies below 40 kg m^{-1} s^{-1} are masked out.
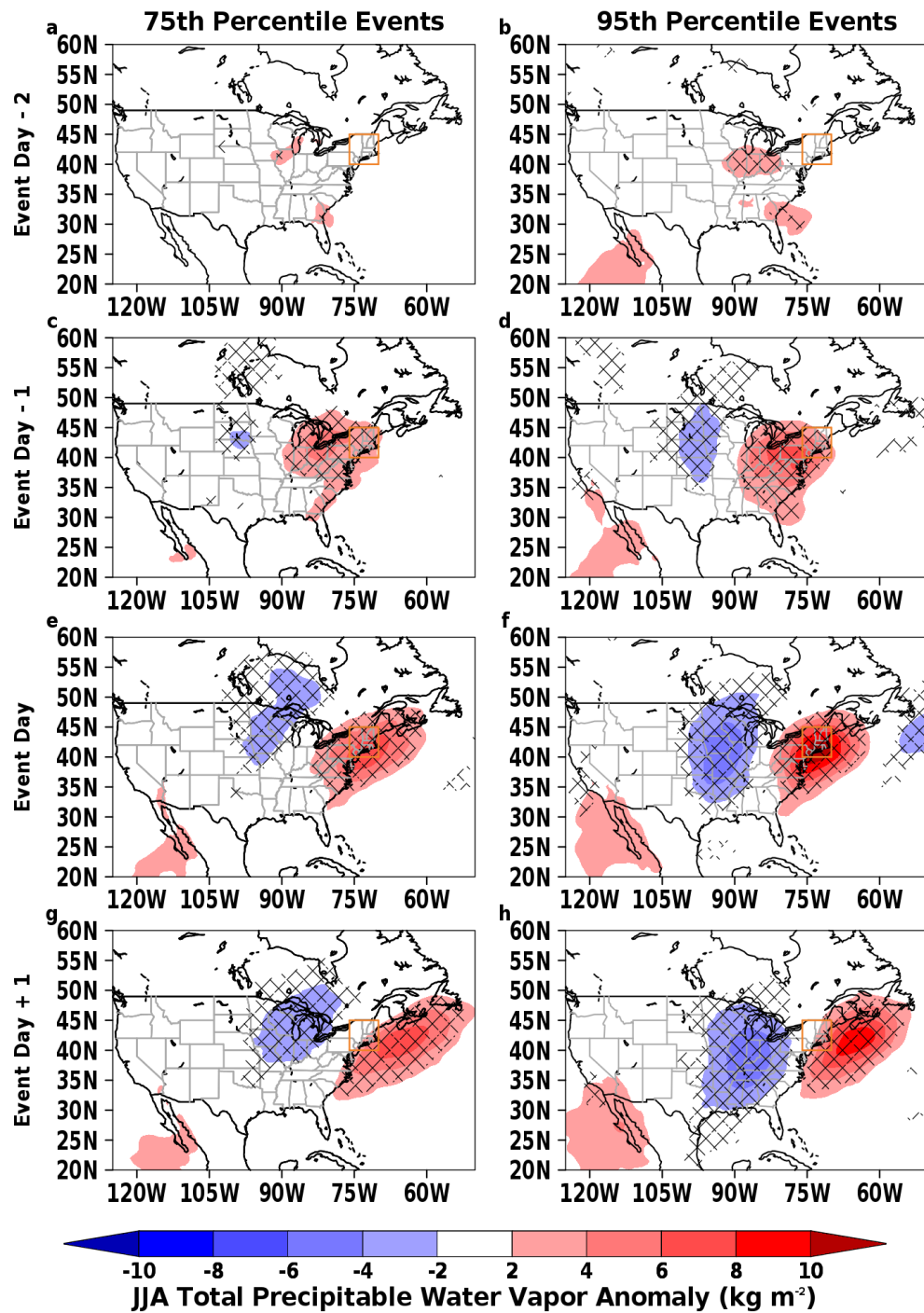
Figure 6: Total precipitable water vapor anomalies composited from two days prior to one day after an observed 75th (left column) and 95th (right column) percentile precipitation event. Hatching denotes regions with a statistical significance of 95%.
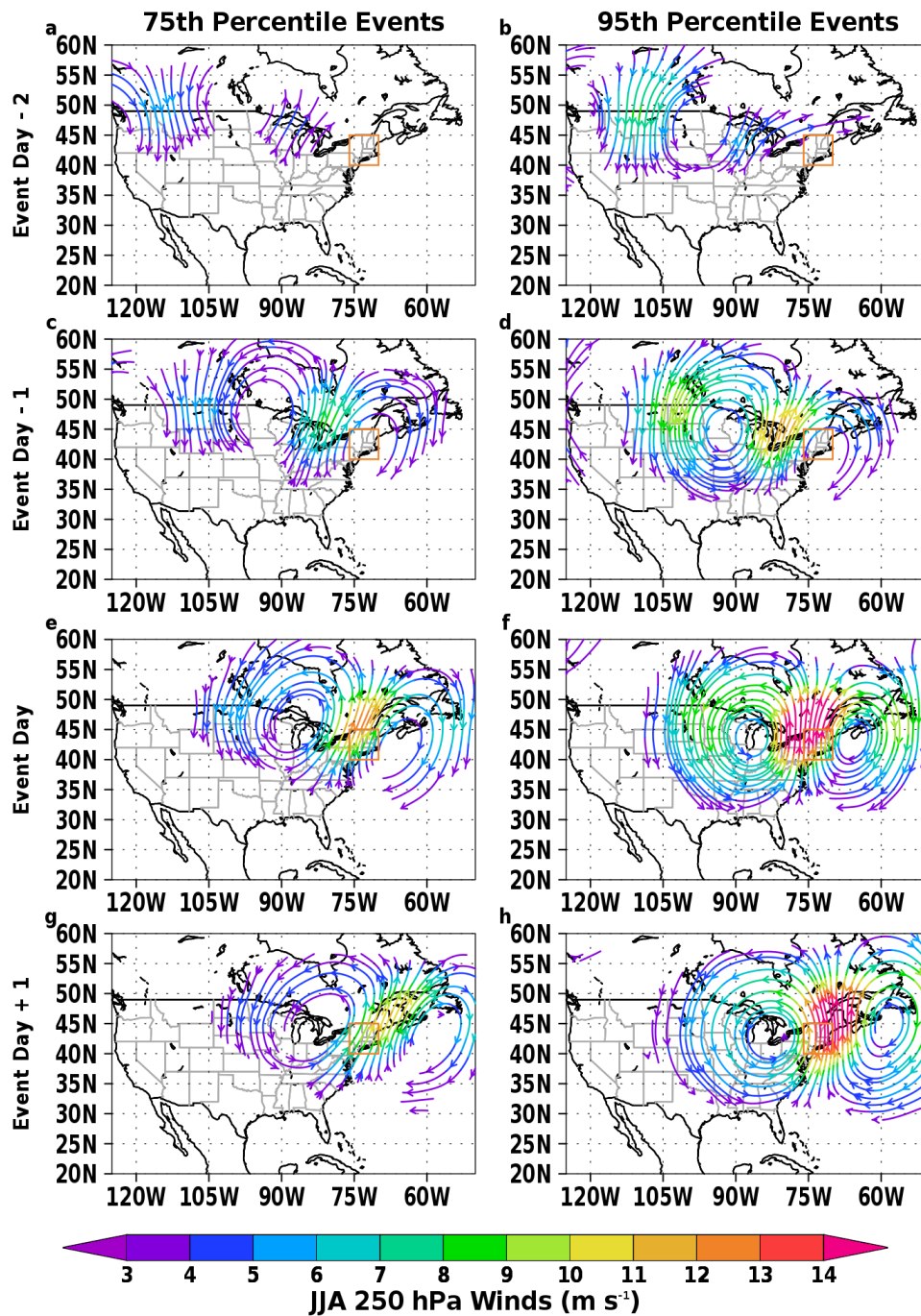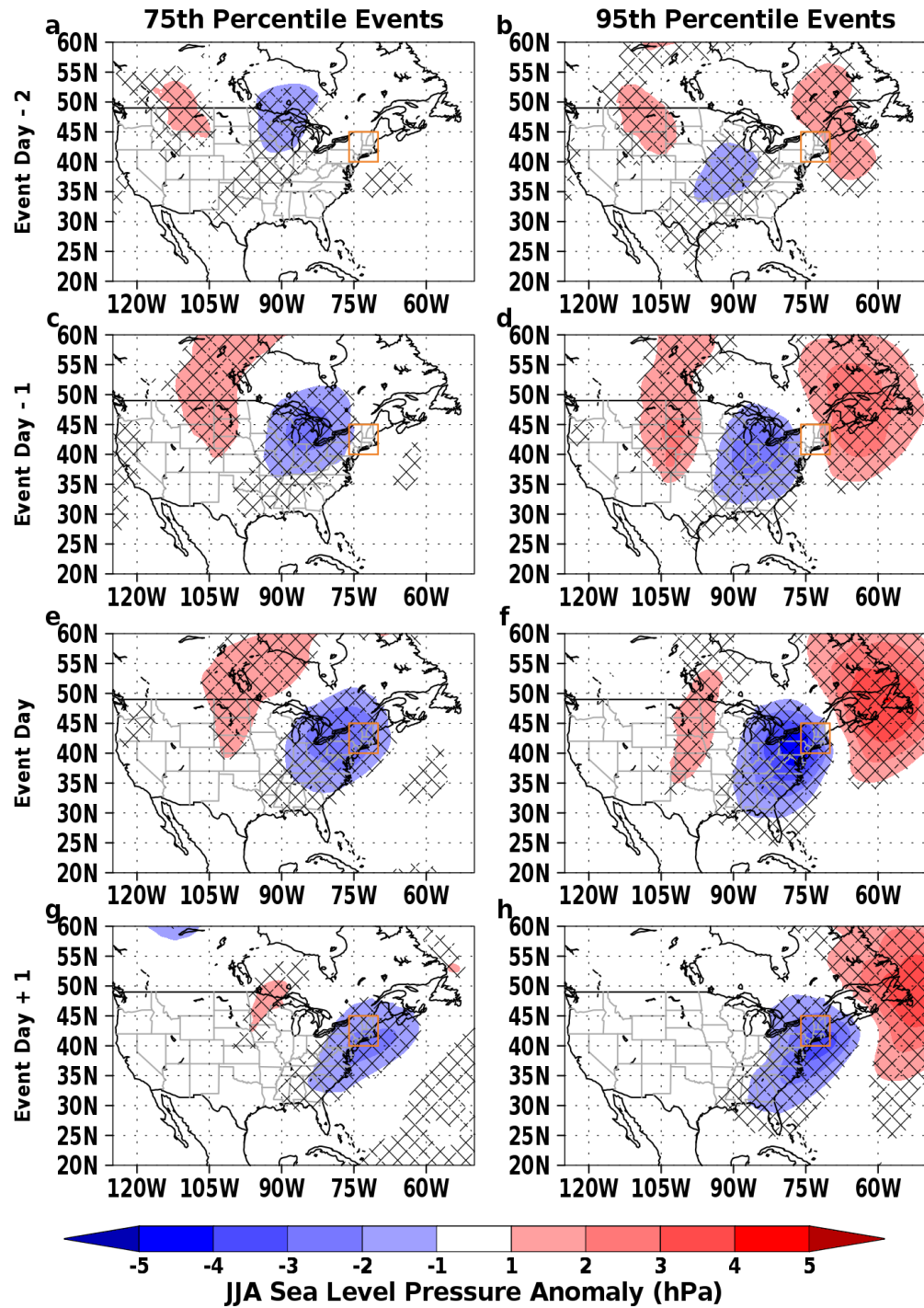
Figure 7: 250 hPa wind anomalies composited from two days prior to one day after an observed

75th (left column) and 95th (right column) percentile precipitation event. Anomalies below

3 m s^{-1} are masked out.

Figure 8: 500 hPa height anomalies composited from two days prior to one day after an observed 75th (left column) and 95th (right column) percentile precipitation event. Hatching denotes regions with a statistical significance of 95%.

Figure 9: Sea level pressure anomalies composited from two days prior to one day after an observed 75th (left column) and 95th (right column) percentile precipitation event. Hatching denotes regions with a statistical significance of 95%.
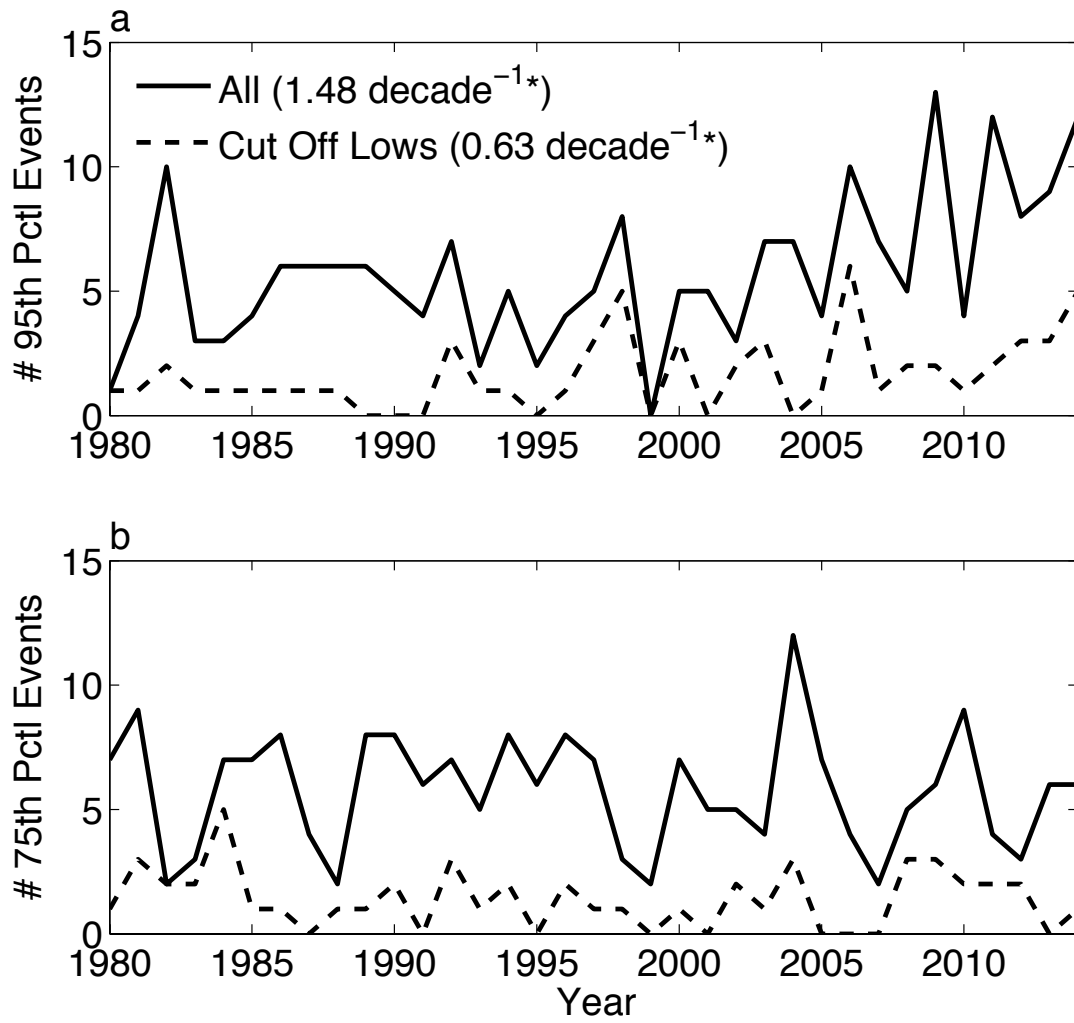
667

668   Figure 10: Time series of the total number of extreme events and the number caused by a cut off

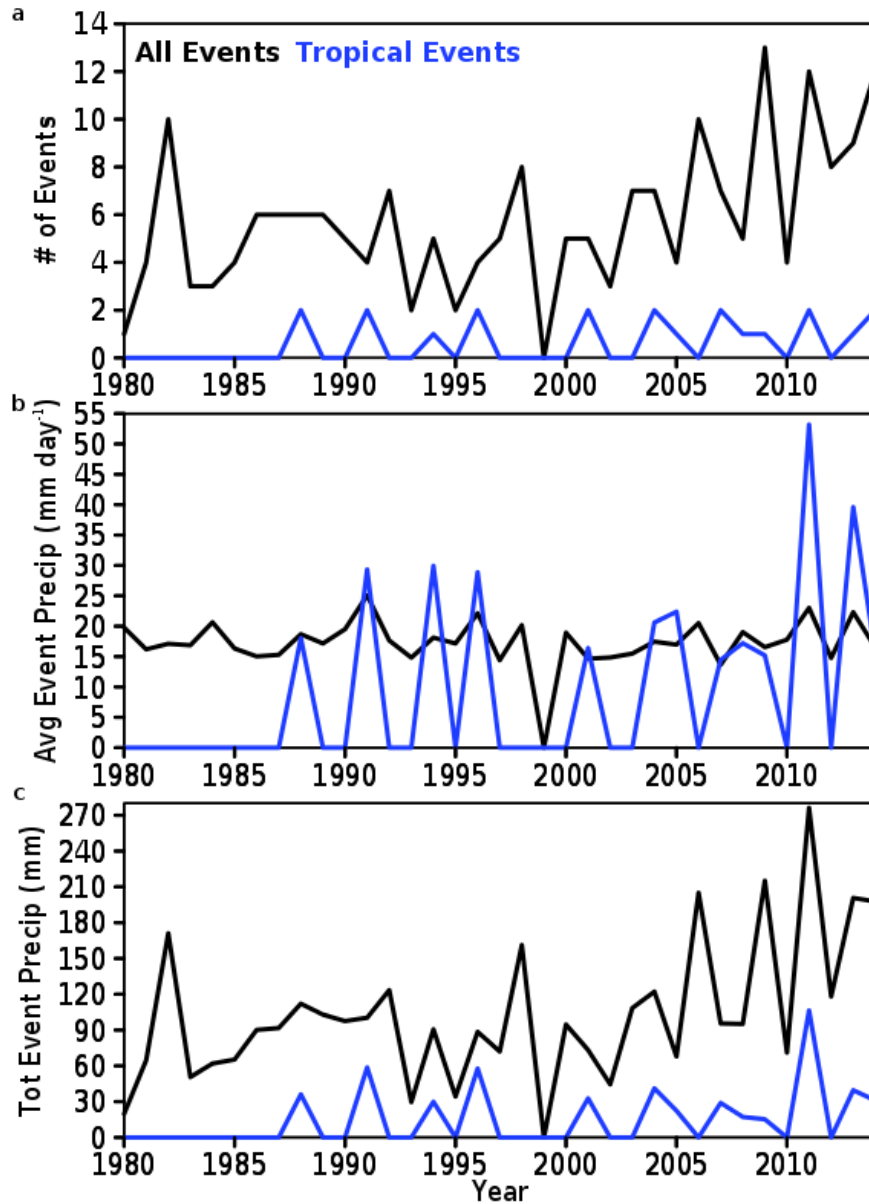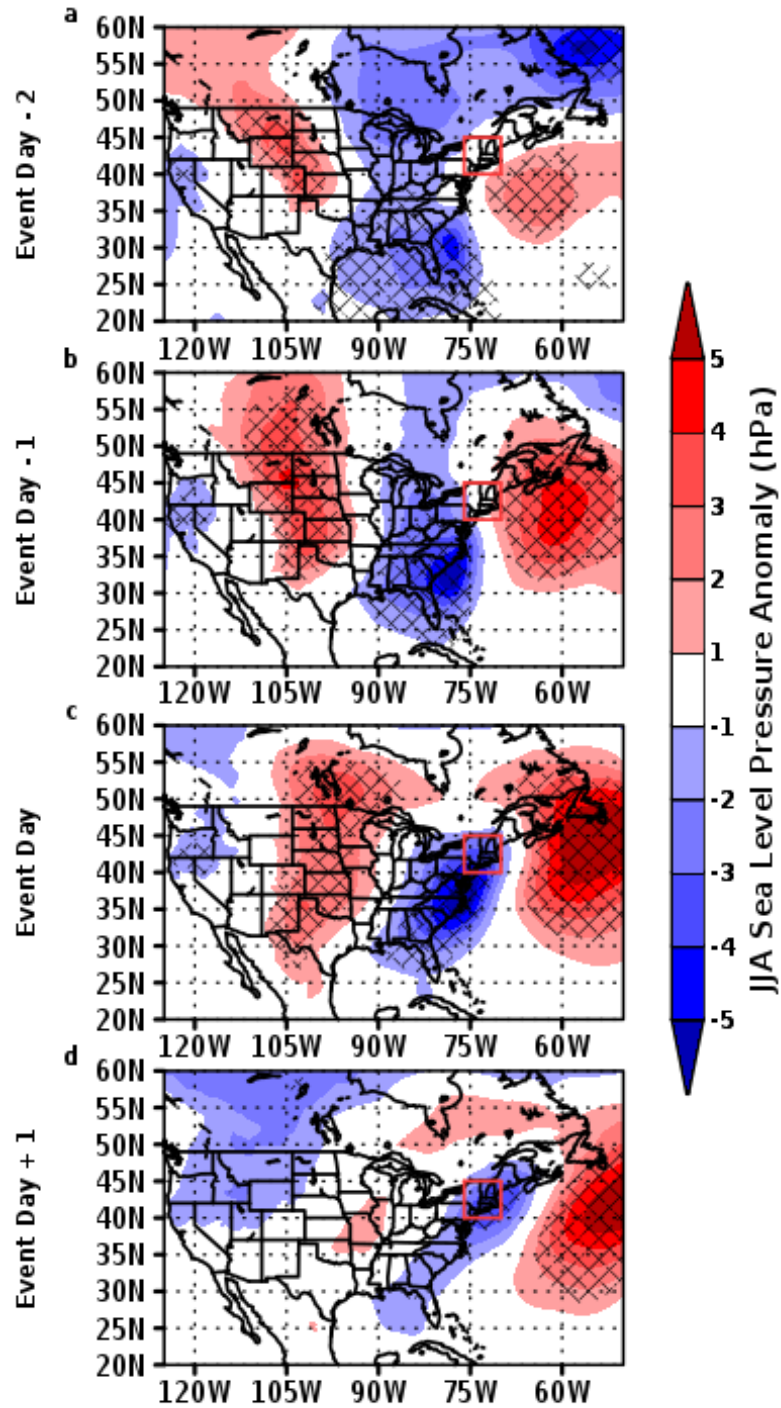669   low for the (a) 95th percentile and (b) 75th percentile.

Figure 11: (a) Time series of number of total and tropical 95th percentile events in the Northeast during June, July, and August. (b) Time series of the average intensity of a 95th percentile event in the Northeast during June, July, and August. (c) Time series of the total amount of precipitation from a 95th percentile event for all events and those caused by a tropical cyclone in the Northeast during June, July, and August.

Figure 12: Sea level pressure anomalies composited from two days prior to one day after a 95th percentile precipitation event caused by a tropical cyclone. Hatching denotes regions with a statistical significance of 95%.
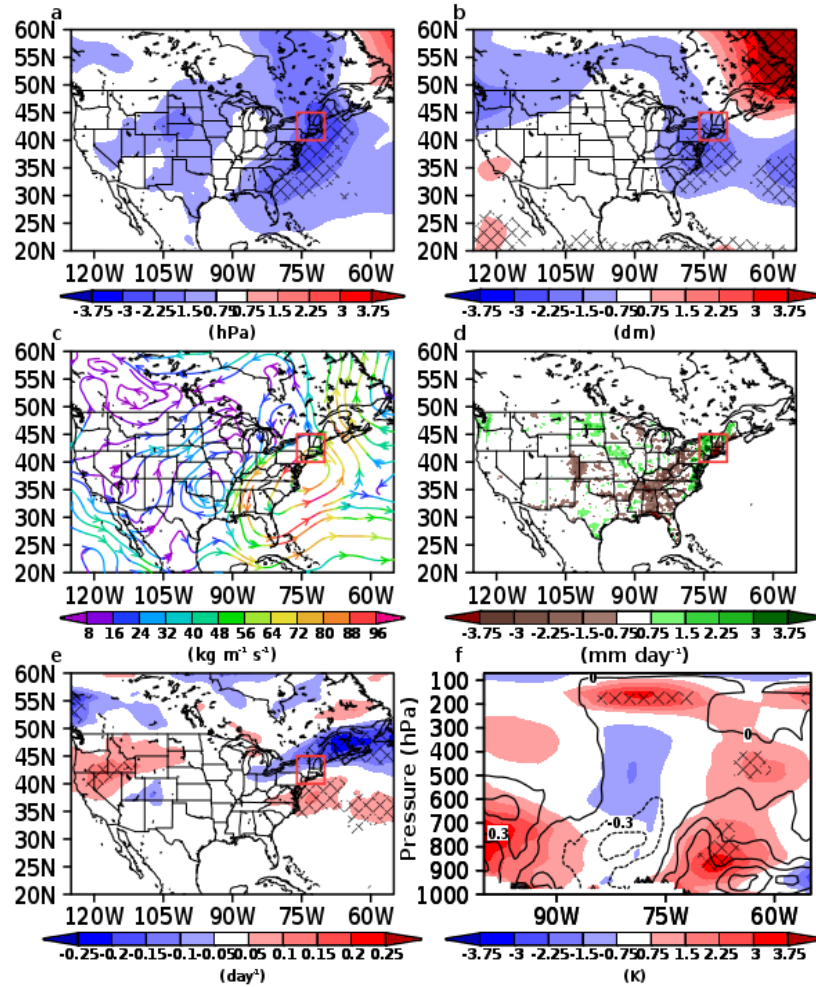
681

682 Figure 13: The difference in (a) sea level pressure, (b) 500 hPa height, (c) vertically integrated

683 moisture flux, (d) observed precipitation, (e) Eady growth rate, and (f) the vertical profile of

684 equivalent potential temperature at 42 N composites during 95th percentile precipitation events

685 calculated by subtracting the mean composite for 1980 through 1996 from the composite for

686 1997 through 2014. Hatching denotes regions with a statistical significance of 95%.

687